Pseudogap regime of a strongly interacting two-dimensional Fermi gas with and without confinement-induced effective range of interactions

Brendan C. Mulkerin ⬤, Xia-Ji Liu, and Hui Hu
Centre for Quantum and Optical Science, Swinburne University of Technology, Melbourne, Victoria 3122, Australia

We investigate theoretically the many-body pairing of a strongly correlated two-dimensional Fermi gas with and without negative confinement-induced effective range. Using a strong-coupling effective field theory in the normal state, we show that the specific heat at constant volume can be used as a characteristic indicator of the crossover from the normal Fermi liquid to the pseudogap state in two dimensions. We calculate the pseudogap formation temperature through the specific heat at constant volume, examining the role of a negative confinement-induced effective range on many-body pairing above the superfluid transition. We compare our results with and without effective range to the recent experimental measurement performed with radio-frequency spectroscopy in Murthy *et al.* [P. A. Murthy, M. Neidig, R. Klemt, L. Bayha, I. Boettcher, T. Enss, M. Holten, G. Zürn, P. M. Preiss, and S. Jochim, Science **359**, 452 (2018)]. Although a good qualitative agreement is found, we are not able to discriminate the effect of the confinement-induced effect range in the experimental data.

I. INTRODUCTION

The role of many-body pairing in Fermi systems above the critical superfluid temperature—the so-called pseudogap pairing—is a complex and intriguing problem. It has been long recognized that the pseudogap pairing is important in underpinning superconductivity in high-temperature superconductors [1–3], however due to quantum fluctuations such pairing is difficult to understand [4,5]. The advancement of experimental techniques in trapping and control of interactions in ultracold Fermi gases makes them an ideal platform to study high-temperature many-body pairing across the crossover from a Bose-Einstein condensate (BEC) to a Bardeen-Cooper-Schrieffer (BCS) superfluid [6]. Two-dimensional (2D) ultracold Fermi gases are of particular interest due to the increasingly important role of quantum fluctuations in low dimensions and it is expected that the interaction and temperature regime where pseudogap pairing dominates, known as the pseudogap regime, is much more pronounced [5,7].

Probing the pseudogap regime is difficult as there is no conclusive phase transition across the BEC-BCS crossover. The most widely used theoretical definitions of the pseudogap formation temperature are when a minimum enters the density of states (DOS) or there is a "backbend" in the spectral function [4,5,8–11]. However, there is no uniquely defined transition and these methods can lead to competing formation temperatures. For example, in two dimensions the suppression entering the DOS near the Fermi surface leads to a limit in the weakly interacting BCS regime where pairing and condensation occur at different temperatures. Hence, one has to take a more significant suppression in the DOS to define a consistent and meaningful pseudogap formation temperature [12]. Another technique to observe the effects of many-body pairing is to calculate the equation of state (EOS) and ther-

modynamic properties [13]. It has been observed that the spin susceptibility and specific heat at constant volume contain information about the pairing in a three-dimensional interacting Fermi gas and a characteristic transition temperature can be defined [14]. In this paper we will determine the pseudogap regime using the specific heat at constant volume in two dimensions and compare to the pseudogap regime predicted from the suppression in the DOS (see, e.g., Ref. [12]).

On the experimental side, the advancement of trapping techniques over the last few years has seen a set of important measurements on 2D interacting Fermi gases [15–18]. There was much debate about the pairing regime found in these experiments [12,19,20], where it was argued that the regime probed was not many-body pairing, but two-body pairing. In order for many-body pairing to exist the Fermi gas must have a defined Fermi surface and pairing comes from the many-body nature of the system, which is seen to be true for a chemical potential $\mu > 0$. However, it has also been argued by Ref. [20] that the criterion of a positive chemical potential is too strict and that many-body pairing can exist for a wider interaction and temperature range. Recent experimental work by Murthy *et al.* in Ref. [21] has seemingly observed the high-temperature pairing in 2D Fermi gases for a wide range of interaction strengths and temperatures, although they did not determine a phase diagram.

All previous theoretical methods used to study the pseudogap regime in two dimensions (i.e., *x*-*y* plane) have relied upon a *single* channel model of fermions with a contact interaction. It has been found that this model works very well in explaining experimental data for both below the Berezinskii-Kosterlitz-Thouless (BKT) transition [22–26] and the EOS in the normal state [12,19,20,27–30]. However, recent measurements on the breathing mode and quantum anomaly of 2D Fermi gases [31–33] have found a significant

deviation from the state-of-the-art theoretical prediction using the single-channel model [34,35]. This difference could not be explained through a temperature dependence of the experimental data alone [36], and including higher-order excitations along the z axis of the quasi-2D system is crucial in capturing the reduced breathing mode anomaly [37,38]. Theoretical studies focused on the importance of the quasi-2D nature of scattering and the increased role of confined fermions being able to occupy higher excited single-particle states along the z direction, even when the trapping is extremely tight [38–41]. Including dressed molecules within a two-channel model has been found to effectively describe this situation [38,42], where the molecular state encapsulates the higher excited states and characterizes a confinement-induced effective range of interactions. This highlights the importance of understanding the pseudogap regime by using the two-channel model.

The purpose of this paper is to understand the role played by the confinement-induced effective range on many-body pairing within the two-channel model. Using a field theoretic method to include pairing fluctuations, we calculate the pseudogap formation temperature from the specific heat at constant volume, $\bar{T}$ [14]. We compare this characteristic temperature to the pseudogap temperature determined through a suppression in the DOS at the Fermi surface. We find that when using the definition of the pseudogap temperature, T^*, as a dip in the DOS of 25% of the value at the left fringe, there is a good agreement between T^* and $\bar{T}$ in the weakly interacting regime. We then investigate the role played by the confinement-induced effective range on the pseudogap formation temperature of $\bar{T}$ and see that the effective range shifts the pseudogap window towards weaker binding energies. Finally, we compare our results to the recent radio-frequency (rf) spectroscopy measurements of the pseudogap regime by Murthy *et al.* in Ref. [21], which is the most promising way to experimentally map out the pseudogap regime. For this purpose, we also calculate rf spectra for a trapped system from the analytically continued Green's function, and examine the role of the confinement-induced effective range. A good *qualitative* agreement is found between the experimental data and the theoretical pseudogap regime defined by $\bar{T}$. However, we find that the inclusion of the confinement-induced effective range does not improve the agreement.

The rest of our paper is set out as follows. In Sec. II, we introduce the two-channel model Hamiltonian and outline the many-body T-matrix theory. In Sec. III, we calculate the specific heat at constant volume for a 2D interacting Fermi gas, and using the properties of the specific heat we determine the pseudogap regime and compare it to the pseudogap regime found from the DOS. In Sec. IV, we compare our results to the recent experimental measurements, by calculating the rf spectra and the pseudogap temperature. And finally, in Sec. V, we summarize our findings. For simplicity we set $\hbar = 1$ throughout.

II. HAMILTONIAN

We start our calculation of the many-body Green's function within a two-channel model of the 2D interacting Fermi gas
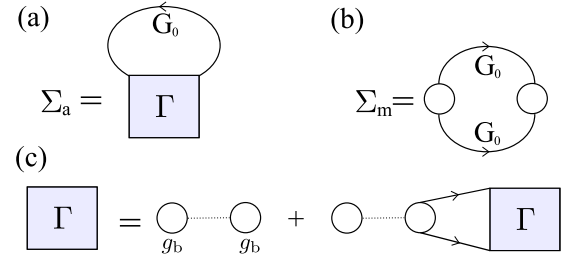

FIG. 1. The Feynman diagrams for (a) the fermion self-energy, (b) the molecular self-energy, and (c) the vertex function within the ladder approximation.

in the normal state, described by the Hamiltonian [43–46]:

$$\mathcal{H} = \sum_{\mathbf{k}\sigma} \xi_{\mathbf{k}} c_{\mathbf{k}\sigma}^{\dagger} c_{\mathbf{k}\sigma} + \sum_{\mathbf{q}} (\epsilon_{\mathbf{q}}/2 + \nu - 2\mu) b_{\mathbf{q}}^{\dagger} b_{\mathbf{q}}$$
$$+ g_{\mathrm{b}} \sum_{\mathbf{kq}} (b_{\mathbf{q}} c_{\mathbf{q}/2+\mathbf{k}\uparrow}^{\dagger} c_{\mathbf{q}/2-\mathbf{k}\downarrow}^{\dagger} + \mathrm{H.c.}), \qquad (1)$$

where H.c. is the Hermitian conjugate, $c_{\mathbf{k}\sigma}$ are the annihilation operators of atoms with spin $\sigma = \uparrow, \downarrow$ and mass M in the open channel, and $b_{\mathbf{q}}$ are the annihilation operators of molecules in the closed channel. The kinetic energy of the Fermi atoms measured from the chemical potential μ is $\xi_{\mathbf{k}} = \epsilon_{\mathbf{k}} - \mu$, where $\epsilon_{\mathbf{k}} = k^2/(2M)$. The threshold energy of the diatomic molecule is ν and the Feshbach coupling is g_{b}. As we have used a momentum-independent Feshbach coupling constant, which is unphysical at the high energy, there is an ultraviolet divergence. This divergence can be removed by renormalizing ν, as we discuss in detail in the Appendix. ν and g_{b} are related to the physical observables of the binding energy ε_B and the effective range of interactions $R_s < 0$ via

$$\nu = -\varepsilon_B + g_{\mathrm{b}}^2 \sum_{\mathbf{k}} \frac{1}{2\epsilon_{\mathbf{k}} + \varepsilon_B}, \qquad (2)$$

$$g_{\mathrm{b}}^2 = -\frac{4\pi \hbar^4}{M^2} \frac{1}{R_s}. \qquad (3)$$

Many-body T-matrix theory

We consider the effect of pair fluctuations on the normal-state properties of a strongly correlated Fermi system through the non-self-consistent T-matrix approximation. The interacting thermal Green's function of fermions at temperature T is given by [9,45,47]

$$G(\mathbf{k}, i\omega_m) = \frac{1}{i\omega_m - (\epsilon_{\mathbf{k}} - \mu) - \Sigma_a(\mathbf{k}, i\omega_m)}, \qquad (4)$$

where we sum all of the ladder-type diagrams to obtain the self-energy [see Fig. 1(a)]:

$$\Sigma_a = k_B T \sum_{\mathbf{q}, i\nu_n} G^{(0)}(\mathbf{q} - \mathbf{k}, i\nu_n - i\omega_m)\Gamma(\mathbf{q}, i\nu_n). \qquad (5)$$

Here, the fermionic and bosonic Matsubara frequencies are, respectively, $\omega_m = (2m + 1)\pi k_B T$ and $\nu_n \equiv 2n\pi k_B T$ for integers m and n, and the free Green's function is $G^{(0)}(\mathbf{k}, i\omega_m) = (i\omega_m - \xi_{\mathbf{k}})^{-1}$. The vertex function $\Gamma(\mathbf{q}, i\nu_n)$, which is an

effective bosonic propagator, can be written through Fig. 1(c):

$$\Gamma^{-1}(\mathbf{q}, i\nu_n) = U_{\text{eff}}^{-1}(\mathbf{q}, i\nu_n) + \Pi(\mathbf{q}, i\nu_n), \quad (6)$$

with the effective interaction $U_{\text{eff}} \equiv g_b^2 D_0(\mathbf{q}, i\nu_n)$ and the pair propagator $\Pi(\mathbf{q}, i\nu_n)$:

$$\Pi = k_B T \sum_{\mathbf{k}, i\omega_m} G^{(0)}(\mathbf{q} - \mathbf{k}, i\nu_n - i\omega_m) G^{(0)}(\mathbf{k}, i\omega_m)$$

$$= \sum_{\mathbf{k}, i\omega_m} \frac{1 - f\left(\xi_{\frac{\mathbf{q}}{2} - \mathbf{k}}\right) - f\left(\xi_{\frac{\mathbf{q}}{2} + \mathbf{k}}\right)}{2\epsilon_{\mathbf{k}} - 2\mu + \epsilon_{\mathbf{q}}/2 - i\nu_n}. \quad (7)$$

Here, the free Green's function of a molecular boson is $D_0(\mathbf{q}, i\nu_n) = 1/[i\nu_n - \epsilon_{\mathbf{q}}^{B}]$ with dispersion $\epsilon_{\mathbf{q}}^{B} = \epsilon_{\mathbf{q}}/2 - \nu + 2\mu$. As shown in Fig. 1(b), similar to the fermionic Green's function, the interacting Green's function of the molecular boson also includes a self-energy correction:

$$D(\mathbf{q}, i\nu_n) = \frac{1}{i\nu_n - \epsilon_{\mathbf{q}}/2 - \nu + 2\mu - \Sigma_{\text{m}}(\mathbf{q}, i\nu_n)}, \quad (8)$$

where $\Sigma_{\text{m}}(\mathbf{q}, i\nu_n)$ is given by

$$\Sigma_{\text{m}} = -g_b^2 \Pi(\mathbf{q}, i\nu_n). \quad (9)$$

At a given temperature, binding energy, and effective range we tune the chemical potential to satisfy the particle number equation:

$$N = N_a + 2N_m$$

$$= 2k_B T \sum_{\mathbf{k}, i\omega_m} G(\mathbf{k}, i\omega_m) - 2k_B T \sum_{\mathbf{q}, i\nu_n} D(\mathbf{q}, i\nu_n). \quad (10)$$

To make the equations dimensionless, we define the Fermi units $k_F = (2\pi n)^{1/2}$, $\varepsilon_F = k_F^2/(2M)$, and $T_F = \varepsilon_F/k_B$, where $n = N/V = k_F^2/2\pi$ is the total density and V is the area (or the volume in two dimensions). We then converge the chemical potential μ/ε_F at a given reduced temperature T/T_F, binding energy $\varepsilon_B/\varepsilon_F$, and effective range $k_F^2 R_s$.

The closed set of Eqs. (4)–(9) can be solved directly with a numerical sum over the Matsubara frequencies, as done in Ref. [47]; however, within this methodology it is difficult to numerically continue the thermal Green's function to the real axis, which is needed for obtaining the spectral function and the DOS. Alternatively, we can analytically continue the Matsubara frequencies to the real axis first, allowing us to directly calculate the analytically continued Green's function [20,48,49]. The thermal Green's function then becomes

$$G(\mathbf{k}, \omega^+) = \frac{1}{\omega^+ - (\epsilon_{\mathbf{k}} - \mu) - \Sigma_a(\mathbf{k}, \omega^+)}, \quad (11)$$

where $\omega^+ \equiv \omega + i0^+$. Using contour integration the self-energy function takes the form [50]

$$\Sigma_a(\mathbf{k}, \omega^+)$$
$$= \int \frac{d\mathbf{q}}{(2\pi)^2} \frac{d\epsilon}{\pi} [b(\epsilon) G^{(0)}(\mathbf{k} - \mathbf{q}, \epsilon - \omega^+) \text{Im}\Gamma(\mathbf{q}, \epsilon^+)$$
$$- f(\epsilon) \text{Im}G^{(0)}(\mathbf{k}, \epsilon^+)\Gamma(\mathbf{k} + \mathbf{q}, \epsilon + \omega^+)], \quad (12)$$

where $f(z) = [\exp(\beta z) + 1]^{-1}$ and $b(z) = [\exp(\beta z) - 1]^{-1}$ are the Fermi and Bose distributions, respectively, with $\beta \equiv$

$1/(k_B T)$. We then find the imaginary part of the analytically continued self-energy,

$$\text{Im}[\Sigma_a(\mathbf{k}, \omega)] = \int \frac{d\mathbf{q}}{(2\pi)^2} \frac{d\epsilon}{2\pi} [b(\epsilon) + f(\epsilon - \omega)]$$
$$\times \text{Im}\Gamma(\mathbf{q}, \epsilon) \text{Im}G^{(0)}(\mathbf{q} - \mathbf{k}, \epsilon - \omega), \quad (13)$$

and we calculate the real part of the self-energy from the Kramers-Kronig relation:

$$\text{Re}[\Sigma_a(\mathbf{k}, \omega)] = \frac{1}{\pi} \mathcal{P} \int_{-\infty}^{\infty} d\omega' \frac{\text{Im}[\Sigma_a(\mathbf{k}, \omega')]}{\omega' - \omega}. \quad (14)$$

The DOS is calculated by analytically continuing the fermionic Green's function and integrating over the momenta:

$$\rho(\omega) = -\frac{1}{\pi} \sum_{\mathbf{k}} \text{Im}G(\mathbf{k}, i\omega_m \to \omega + i0^+)$$

$$\equiv \sum_{\mathbf{k}} A(\mathbf{k}, \omega). \quad (15)$$

It is possible to relate the above many-body T-matrix theory to the Nozieres–Schmitt-Rink (NSR) [36,51] approach by truncating the self-energy to the first order, i.e.,

$$G(\mathbf{k}, i\omega_m) = G_0(\mathbf{k}, i\omega_m)$$
$$+ G_0(\mathbf{k}, i\omega_m)\Sigma_a(\mathbf{k}, i\omega_m)G_0(\mathbf{k}, i\omega_m). \quad (16)$$

This is equivalent to writing the thermodynamic potential for a two-channel model:

$$\Omega = \Omega_F^{(0)} + \Omega_B^{(0)} - \sum_{\mathbf{q}, i\nu_n} \ln\left[1 + g_b^2 D_0 \Pi(\mathbf{q}, i\nu_n)\right], \quad (17)$$

where $\Omega_F^{(0)} = 2 \sum_{\mathbf{k}} \ln(e^{-\beta\epsilon_{\mathbf{k}}} + 1)$ is the free fermionic thermodynamic potential and $\Omega_B^{(0)} = \sum_{\mathbf{q}} \ln(e^{-\beta\epsilon_{\mathbf{q}}^{B}} - 1)$ is the free bosonic thermodynamic potential. Although the pressure EOS and thermodynamic properties can be calculated from the density equation of state in Eq. (10) via the Gibbs-Duhem relation [12,28], we use the NSR approach for the calculation of the specific heat at constant volume as this is considerably simpler: it is more feasible to calculate numerically the derivatives with respect to the chemical potential and interaction strength. We expect that there is a small correction to the specific heat at constant volume when the self-energy becomes more significant and the approximation of Eq. (16) weakens.

Through the thermodynamic potential we can calculate the thermodynamic properties of the system, starting with the pressure EOS $P = \Omega/V$, the energy $E = -TS + \Omega + \mu N$, and the entropy $S = -(\partial\Omega/\partial T)_\mu$ [46]. The specific heat at constant volume is given by

$$C_V = \left(\frac{\partial E}{\partial T}\right)_{V,N}. \quad (18)$$

For the specific heat at constant volume it is simplest to calculate the derivative of the energy with respect to temperature numerically:

$$C_V = \frac{E[\mu(T+\delta), T+\delta] - E[\mu(T-\delta), T-\delta]}{2\delta}, \quad (19)$$

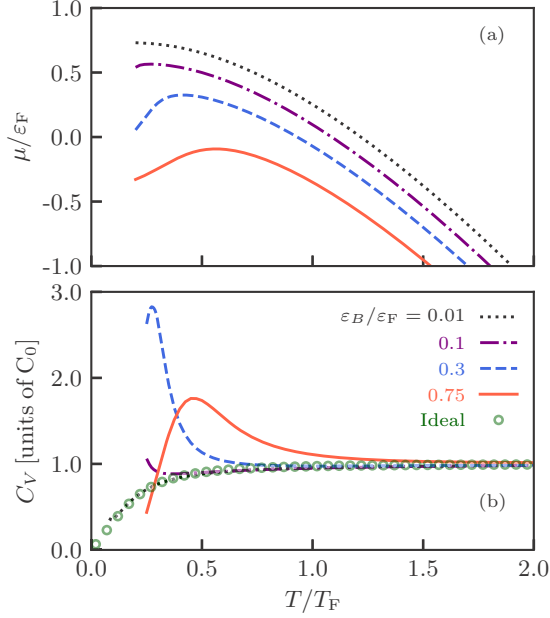where we set $\delta = 0.01 T_F$ [14].

FIG. 2. (a) The chemical potential in units of the Fermi energy for binding energies $\varepsilon_B/\varepsilon_F = 0.01$ (black dotted), 0.1 (purple dot-dashed), 0.3 (blue dashed), and 0.75 (red solid) and (b) the specific heat at constant volume in units of $C_0 = Nk_B$ as a function of reduced temperature for the same binding energies. The ideal Fermi gas specific heat predicted by Eq. (20) is shown as the symbols.

We note that since the superfluid transition temperature predicted by the Thouless criterion is precisely zero in two dimensions [1,52] we do not consider the finite-temperature transition in this paper. It is also important to note the limitations and benefits of the non-self-consistent T-matrix scheme. This T-matrix scheme is useful as it is possible to analytically continue the Green's function and directly obtain spectral functions: we do not rely on a numerically unsound procedure. The non-self-consistent T-matrix approximation is well defined and works well in the high-temperature regime where the interaction strength effectively becomes weaker, in the tightly bound limit where the binding energy $\epsilon_B \gg \varepsilon_F$ and molecules are well formed, or in the weakly interacting limit where the binding energy is exponentially small. However, when the interactions between performed molecules are strong, such as in the strongly correlated regime and at sufficiently low temperatures, the chemical potential approaches the binding energy and we expect the non-self-consistent T-matrix theory to give incorrect results [29]. In this paper we avoid this problem as we focus on the relatively high-temperature regime (i.e., at temperatures larger than a characteristic BKT temperature of $\approx 0.1T_F$).

III. RESULTS

A. Specific heat

We first consider the broad resonance limit and let $g_b \rightarrow \infty$, i.e., $k_F^2 R_s = 0$, in order to understand the general properties of the specific heat at constant volume. Figure 2(a) shows the reduced chemical potential in units of the Fermi energy as a function of temperature, T/T_F. We see that the temperature

dependence of the chemical potential for each binding energy is nontrivial, and as we go towards the strongly correlated and low-temperature regime we see the chemical potential has a maximum value, indicating the tendency of a transition towards the superfluid state.

In Fig. 2(b) we plot the specific heat at constant volume in units of $C_0 = Nk_B$, as a function of temperature from the weakly attractive BCS side to the strongly correlated regime. We see that for the weakest binding energy, $\varepsilon_B/\varepsilon_F = 0.01$, the specific heat is reduced to the ideal Fermi gas specific heat at constant volume:

$$C_V^F = 2\frac{\mathrm{Li}_2(-e^{\beta\mu})}{\mathrm{Li}_1(-e^{\beta\mu})} - \frac{\mathrm{Li}_1(-e^{\beta\mu})}{\mathrm{Li}_0(-e^{\beta\mu})}. \tag{20}$$

In the high-temperature limit (i.e., $T > T_F$), the specific heat for all interactions is approaching $C_V = Nk_B$. In the relatively high-temperature regime (i.e., $T \sim 0.3T_F$), the specific heat is enhanced compared to the ideal gas result, and typically exhibits a peak structure. As we move from the weakly attractive regime to the strongly coupled regime, the enhancement or peak first increases and then decreases. As we shall discuss in greater detail below, this enhancement connects to the many-body pseudogap pairing. Before doing so, let us briefly review the DOS, which provides a conventional characterization of the pseudogap regime.

B. Density of states

Indeed, it has been discussed in a range of works that in both two and three dimensions the DOS can be used to find the pseudogap formation temperature [5]. In Fig. 3 we plot the DOS at the interaction strength $\varepsilon_B/\varepsilon_F = 0.3$ for a range of temperatures, normalized by the ideal density of states, $\rho_0 = m/\pi$, and showing the evolution of the suppression, or dip, near zero frequency with respect to the chemical potential. It is readily seen that, as the temperature reduces, the suppression in the density of states increases. In this paper we choose to take the pseudogap formation temperature T^* when there is a significant dip near the Fermi surface [12], that is, when the lowest value near $\omega/\varepsilon_F \simeq 0$ is 25% lower than the left peak value. In this way, we can approach the BKT transition temperature in the weakly interacting regime, and as
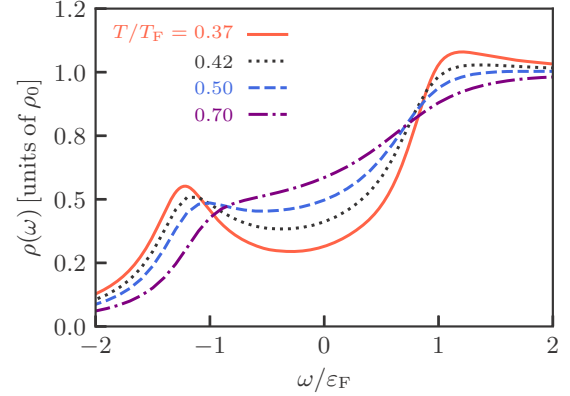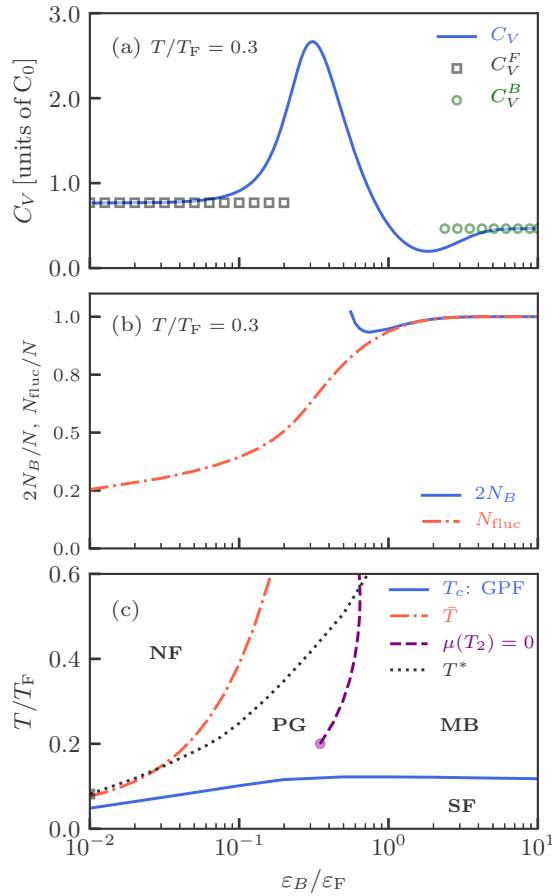

FIG. 3. The density of states is plotted as a function of frequency in units of $\rho_0 = m/\pi$ for an interaction strength of $\varepsilon_B/\varepsilon_F = 0.3$ and a range of temperatures.

FIG. 4. (a) The specific heat at constant volume in units of $C_0 = Nk_B$ as a function of binding energy $\varepsilon_B/\varepsilon_F$. The Fermi and Bose ideal limits are shown as square and circular symbols, respectively. (b) The fluctuation contribution to the number equation, $N_{\text{fluc}} = -\partial\Omega_{\text{NSR}}/\partial\mu$ (red dot-dashed), and twice the number N_B of stable molecules (blue solid). (c) Phase diagram of the 2D Fermi gas plotted as a function of binding energy and reduced temperature. Crossover to many-body pairing (PG) from the the normal Fermi gas (NF) found from C_V is given by $\bar{T}$ (red dot-dashed). T^* (black dashed) is the pseudogap formation temperature found from the density of states. T_c (blue solid) defines the BKT transition to a superfluid (SF) and is given by the Gaussian pair fluctuation theory in Ref. [25]. The temperature T_2 where $\mu(T_2) = 0$ (purple dashed) is the crossover temperature towards a two-body dominated regime.

the temperature is lowered the system will move directly from a normal Fermi liquid to a superfluid.

C. Phase diagram

To understand the enhancement of the specific heat at constant volume in the relatively high-temperature regime we plot in Fig. 4(a) C_V as a function of binding energy at a fixed temperature $T/T_F = 0.3$. We see there is a clear enhancement of C_V peaked at binding energy $\varepsilon_B/\varepsilon_F \simeq 0.3$, indicating that in this regime there are high-temperature many-body Cooper pairs forming. The specific heat smoothly evolves from an ideal Fermi gas C_V^F on the weakly attractive BCS side to an ideal Bose gas C_V^B of mass $2M$ and density $N/2$ on the strongly attractive BEC side. Here, the ideal Bose gas specific

heat at constant volume takes the same form as in Eq. (20) [53]; however, the chemical potential is determined using the number equation for an equivalent Bose system with mass $2M$ and density $N/2$.

To see how these many-body pairs arise, we plot in Fig. 4(b) the fluctuation contribution to the total number density, $N_{\text{fluc}} = -\partial\Omega_{\text{NSR}}/\partial\mu$, as a function of the binding energy (red dot-dashed line), where

$$\Omega_{\text{NSR}} = -\frac{1}{\pi}\sum_{\mathbf{q}}\int_{-\infty}^{\infty}\frac{d\omega}{e^{\beta\omega}-1}\delta(\mathbf{q},\omega), \qquad (21)$$

and $\delta(\mathbf{q},\omega) \equiv -\text{Im}\ln[-\Gamma^{-1}(\mathbf{q},\omega+i0^+)]$. The contribution of N_{fluc} to the total density can be thought of as renormalized Cooper-pair fluctuation and can be broken into contributions from metastable pairs and scattered states [43,54]. In particular, if there is no Fermi surface and the chemical potential is negative, i.e., $\mu < 0$, it is possible to divide the fluctuation contribution into twice the number of stable molecules N_B (blue solid line) and of scattered states N_{sc} (not shown in the figure) [14,43]. We plot in Fig. 4(b) twice the number of stable molecules N_B for binding energies greater than $\varepsilon_B/\varepsilon_F > 0.5$, where N_B can be calculated from the bound-state contribution [55]. For binding energies below this value the chemical potential is positive and the stable molecule formulation is unphysical. Thus, it is clear that the contribution of pairs below binding energies $\varepsilon_B/\varepsilon_F \sim 0.5$ should be from many-body pairing and gives rise to the enhancement of the specific heat at constant volume C_V.

Following the idea of Ref. [14] we take the minimal value of $C_V(T/T_F)$ as a characteristic transition temperature, $\bar{T}$, between the normal Fermi gas and a many-body paired system, i.e., the pseudogap regime. This value signifies the deviation from the ideal C_V in the weakly attractive regime, and breaks down as we approach strongly attractive interactions, and can be seen as the minimum value in Fig. 2, for temperatures above which the chemical potential is unphysically tending towards the binding energy. This is not a true transition temperature to the pseudogap regime but a characteristic transition.

We plot a phase diagram in Fig. 4(c) showing the crossover temperature to the pseudogap regime defined by $\bar{T}$ (red dot-dashed) and T^* (black dotted), and the BKT transition temperature T_c to a superfluid found by the Gaussian pair fluctuation theory in Ref. [25] (blue solid). We show also the crossover line to a regime dominated by two-body physics by the curve $\mu(T_2) = 0$ (purple dashed). This line bounds the pseudogap regime as we increase the binding energy. All together, the three lines of the characteristic temperatures, $\bar{T}$, T_c, and T_2, enclose a pseudogap regime. We note that the calculation of $\mu(T_2) = 0$ is stopped for temperatures below $T/T_F = 0.2$ due to the breakdown of the NSR and T-matrix schemes.

D. Effective range dependence

We now move to consider the confinement-induced effective range dependence of the density of state, specific heat at constant volume, and pseudogap formation temperature. We first show the density of states in Fig. 5 normalized by the ideal density of states $\rho_0 = m/\pi$, for two temperatures (a)
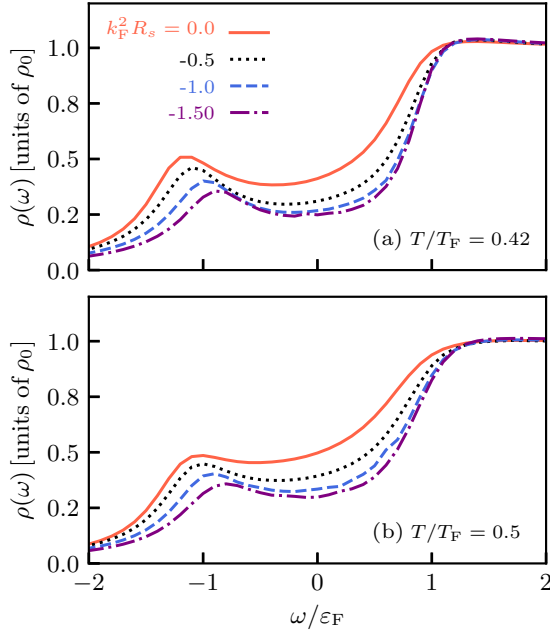
FIG. 5. The density of states is plotted as a function of frequency in units of $\rho_0 = m/\pi$ for an interaction strength of $\varepsilon_B/\varepsilon_F = 0.3$, temperatures (a) $T/T_F = 0.42$ and (b) $T/T_F = 0.5$, and for negative effective ranges $k_F^2 R_s = 0$ to -1.5.
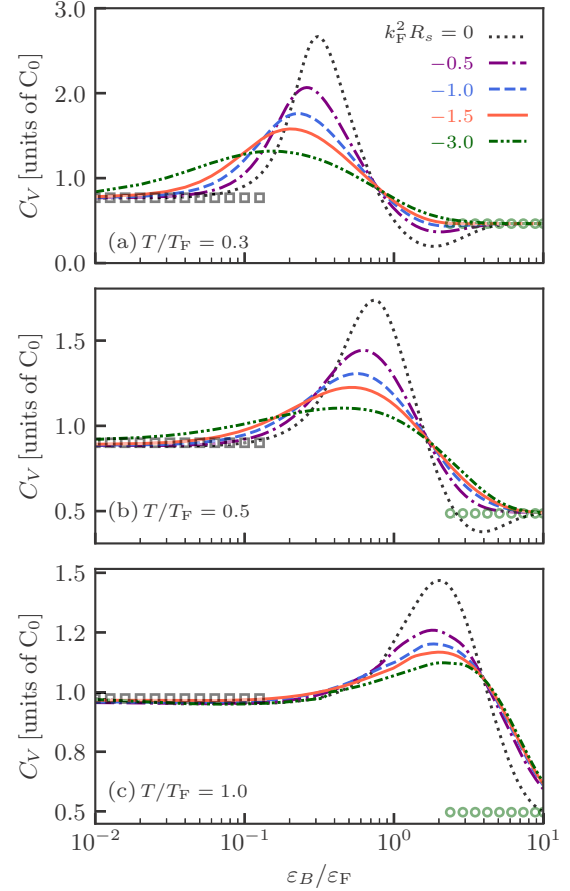

FIG. 6. The specific heat at constant volume in units of $C_0 = Nk_B$ as a function of interaction strength $\varepsilon_b/\varepsilon_F$ for negative effective ranges: $k_F^2 R_s = 0$ (black dotted), $k_F^2 R_s = -0.5$ (purple dot-dashed), $k_F^2 R_s = -1.0$ (blue dashed), $k_F^2 R_s = -1.5$ (red solid), and $k_F^2 R_s = -3.0$ (green dot-dot-dashed), for temperatures (a) $T/T_F = 0.3$, (b) $T/T_F = 0.5$, and (c) $T/T_F = 1.0$.

$T/T_F = 0.42$ and (b) $T/T_F = 0.5$, at fixed interaction strength $\varepsilon_B/\varepsilon_F = 0.3$, and negative effective ranges $k_F^2 R_s = 0$ to -1.5. As the negative effective range increases in absolute value we see the suppression near zero frequency with respect to the chemical potential lower for both temperatures. This is indicating that for large $|k_F^2 R_s|$ the transition to the pseudogap will occur at higher temperatures.

To clearly understand the role of effective range on the pseudogap we show C_V in Fig. 6 as a function of binding energy, $\varepsilon_B/\varepsilon_F$, for negative effective ranges $k_F^2 R_s = 0$ to -3 and temperatures (a) $T/T_F = 0.3$, (b) $T/T_F = 0.5$, and (c) $T/T_F = 1.0$.

The behavior of C_V as a function of increasing effective range in absolute value is nontrivial: we find that the enhancement in the middle interaction regime (around $\varepsilon_B/\varepsilon_F \simeq 0.3$) dampens for each temperature, as the negative effective range increases in absolute value. This is most likely due to the system more readily forming bound molecules with increasing effective range in absolute value. For increasing temperature the peak value is also decreasing, and this is to be expected, as for higher temperatures the role of many-body pairing decreases. We also see that the peak value shifts to larger binding energies at high temperatures as the effective range increases in absolute value, due to a nontrivial competition of pair formation with increasing effective range in absolute value and high temperatures. Furthermore, in the weakly attractive ($\varepsilon_B/\varepsilon_F < 0.1$) and tightly bound ($\varepsilon_B/\varepsilon_F > 5$) limits, the specific heat at constant volume more slowly approaches the ideal gas limits, as $k_F R_s \to -\infty$.

Following the same method to define a pseudogap transition temperature $\bar{T}$ as in Fig. 4, we calculate the effective range dependence of the pseudogap formation and report this

main result of our paper in Fig. 7. The effective ranges are $k_F^2 R_s = 0$ (black dot-dashed), $k_F^2 R_s = -0.5$ (purple dashed), $k_F^2 R_s = -1.0$ (blue dotted), and $k_F^2 R_s = -2$ (red solid). We also plot the crossover temperature T_2 to a molecule dominated system defined by $\mu(T_2) = 0$ using different symbols but the same color for each effective range. The effective range shifts the pseudogap region to weaker binding energies. This is due to the fact that the system more readily forms molecular states with increasing effective range in absolute value, which is seen in Fig. 6(a) as the peak value shifts to weaker binding energies with increasing effective range in absolute value. The interaction window where the pseudogap regime exists remains approximately the same size; however, for the smallest effective range ($k_F^2 R_s = -2$) in the figure, the pseudogap formation temperature is still large for weak interactions. We can see this effect in Fig. 6(a), where for increasing effective range in absolute value and decreasing binding energy C_V is more slowly approaching the ideal gas result.

IV. COMPARISON TO THE EXPERIMENT

In this section we outline how to compare our two-channel calculations to the recent experimental
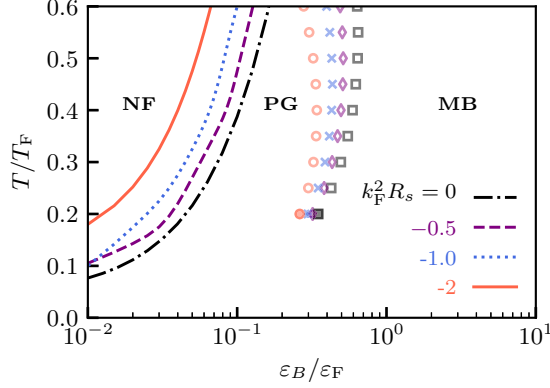
FIG. 7. The pseudogap formation temperature $\bar{T}$ found from the specific heat for negative effective ranges $k_F^2 R_s = 0$ (black dot-dashed), $k_F^2 R_s = -0.5$ (purple dashed), $k_F^2 R_s = -1.0$ (blue dotted), and $k_F^2 R_s = -2$ (red solid). We also show the characteristic temperature T_2 defined by $\mu(T_2) = 0$ using different symbols. At the same effective range, the color is the same for lines ($\bar{T}$) and symbols (T_2).

observations of Murthy *et al.* in Ref. [21], with and without the confinement-induced effective range. For this purpose, we include the effect of an inhomogeneous trap through the local density approximation, $\mu(\mathbf{r}) = \mu_g - \frac{1}{2}M\omega^2\mathbf{r}^2$, where μ_g is the global chemical potential, ω is the trap frequency, and $\mathbf{r}$ is the distance from the center of the trap. We denote the dimensionless radii as $\tilde{r} \equiv r/R_{\text{TF}}$, $R_{\text{TF}}^2 = 2k_B T_F/(m\omega^2)$ is the Thomas-Fermi radius for a zero-temperature noninteracting trapped Fermi gas, and the trap Fermi energy $E_F = (2N)^{1/2}\omega$. We find the global chemical potential by enforcing that the total number of atoms satisfies $N = \int d\mathbf{r}\, n(\mathbf{r})$ for a *central* interaction strength and reduced temperature, where

$$n(\mathbf{r}) = 2 \int \frac{d\mathbf{k}}{(2\pi)^2} d\omega A(\mathbf{k}, \mathbf{r}, \omega) n_F(\omega), \quad (22)$$

the Fermi distribution is $n_F(\omega) = 1/(1 + e^{-\beta\omega})$, and $A(\mathbf{k}, \mathbf{r}, \omega) = (-1/\pi)\,\text{Im}\,G(\mathbf{k}, \mathbf{r}, \omega + i0^+)$ is the spectral function found from the trap dependent Green's function. The inhomogeneous trap means we have trap dependent temperature $T/T_F(\mathbf{r})$ and interaction $\ln[k_F(\mathbf{r})a_{2D}]$.

The experiment in Ref. [21] measures the local spectral response of a trapped 2D Fermi gas through rf spectroscopy. Rf spectroscopy can give information about the properties of the system, by applying a short rf pulse to flip the spin states from an initial strongly interacting system into a weakly interacting final state and then by measuring the number of transferred atoms. This can then be repeated for a range of detunings of the rf pulse and information about the single-particle properties can be measured. In order to compare the spectra found from the experiment, we calculate the trap dependent rf spectra. When there is no final-state interaction we can take the rf response to be [20,48]

$$I_{\text{rf}}(\omega, \mathbf{r}) = 2 \int \frac{d\mathbf{k}}{(2\pi)^2} f(\xi_{\mathbf{k},\mathbf{r}} - \omega) A(\mathbf{k}, \xi_{\mathbf{k},\mathbf{r}} - \omega), \quad (23)$$

where $\xi_{\mathbf{k},\mathbf{r}} = \epsilon_{\mathbf{k}} - \mu(\mathbf{r})$. As a self-consistent check to our calculation of the rf spectra, we can calculate the number
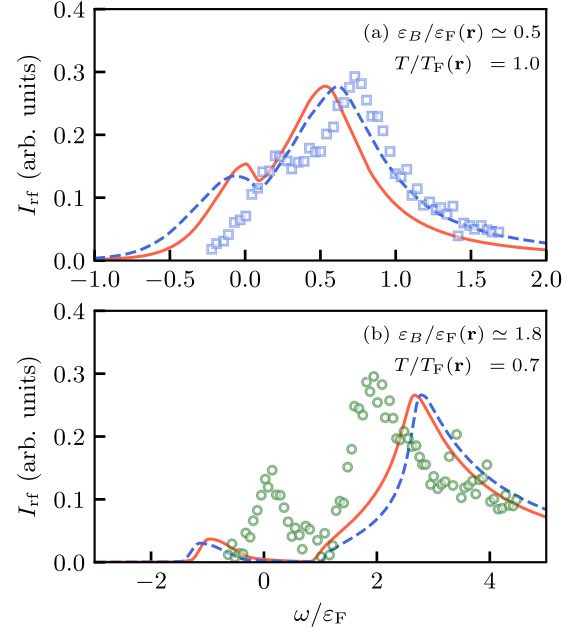

FIG. 8. Comparison of the local spectra from the T matrix (solid lines), with a finite negative effective range (dashed line), and experimental results of Ref. [21] (symbols). We plot the spectra (in arbitrary units) for (a) local temperature $T/T_F = 1.0$ and binding energy $\varepsilon_B/\varepsilon_F \simeq 0.5$ and (b) local temperature $T/T_F = 0.7$ and binding energy $\varepsilon_B/\varepsilon_F \simeq 1.8$.

density, i.e.,

$$N = \int_{-\infty}^{\infty} d\omega \int d\mathbf{r} I_{\text{rf}}(\omega, \mathbf{r}). \quad (24)$$

To compare our two-channel results to the experimental local rf spectra we need to fix a realistic confinement-induced effective range. This can be done as follows. Using the experimentally measured values of the binding energy and Fermi energy we define the ratio $\varepsilon_B/\varepsilon_F$ to obtain the dimensionless effective range for a given interaction. We require that the two-body T matrix $T_{2B}(E^+)$ and the quasi-2D scattering amplitude share the same pole (the same binding energy ε_B) [41]. It is readily seen that the binding energy $\varepsilon_B = \kappa^2/M$ is related to the effective range R_s by

$$R_s = \frac{2\ln(\kappa a_s)}{\kappa^2}, \quad (25)$$

where the 2D scattering length a_s is defined in the Appendix. Using the defined binding energy the dimensionless effective range R_s/a_s^2 and *central* effective range $k_F^2 R_s$ are then found.

In Fig. 8 we plot the rf spectroscopy found from the T-matrix approximation and from Figs. 3(c) and 3(d) of Ref. [21]. We have taken the experimental values of *central* binding energies $\varepsilon_B = 1.37$ kHz in Fig. 8(a) and 9.31 kHz in Fig. 8(b), and Fermi energies $\varepsilon_F = 6.56$ and 7.61 kHz, which correspond to Feshbach resonances of 670 and 690 G at two fixed radii $\mathbf{r}$ as in the experiment corresponding to the measured local trap temperatures of $T/T_F = 1.0$ and 0.7, respectively. This defines a confinement-induced effective range of $R_s/a_s^2 \simeq -0.2$ and -1.2, respectively. Fixing the local temperature we determine the local chemical
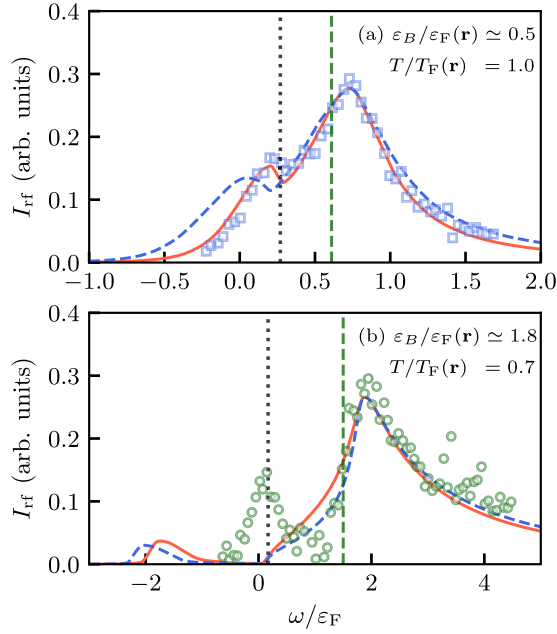
FIG. 9. Comparison of the local spectra from the shifted T matrix (solid lines), with a finite negative effective range (dashed line), and experimental results of Ref. [21] (symbols). We plot the shifted spectra (in arbitrary units) for (a) local temperature $T/T_F = 1.0$ and binding energy $\varepsilon_B/\varepsilon_F \simeq 0.5$ and (b) local temperature $T/T_F = 0.7$ and binding energy $\varepsilon_B/\varepsilon_F \simeq 1.8$. The green dashed lines are the threshold energy and black dotted lines are the free energy, both determined experimentally.

potential, Fermi momenta $k_F^2(\mathbf{r}) \simeq 0.44$ and 0.71, and thus binding energies $\varepsilon_B/\varepsilon_F(\mathbf{r}) \simeq 0.5$ and 1.8, for each Feshbach resonance, respectively. Although there is a realistic effective range in the experiment, for comparison we also show the theoretical predictions without effective range using red solid lines.

Quite generally, there are two peaks in the spectra. The right peak, referred to as the pairing peak, comes from the signal of Cooper pairs. The left peak, referred to as the free peak, is contributed from free, unpaired atoms. The difference between the experimental and theoretical spectra is partially due to the residual final-state effects, which is present in the experiment but is not captured by our theory. We see the difference between theoretical and experimental spectra is larger for stronger binding energy, i.e., in Fig. 8(b). In order to compare theoretical and experimental spectra for determining the ratio between the threshold and free energies and the pseudogap regime we normalize our spectra to have the same peak value for the pairing peak, and shift the peak to have its maximum at the same frequency, as plotted in Fig. 9.

First, the results at smaller binding energy in Fig. 9(a) match quite well for the whole *shifted* spectra when there is *no* finite effective range. Using the same fitting method in Ref. [21] to determine the threshold energy, which is the energy required to break a pair, we find that the threshold and free-peak energies are similar to the experimental values. These experimental values are plotted in Fig. 9(a) using the vertical lines. The ratio of the difference of these energies to the binding energy indicates that we are in the pseudogap

regime for this interaction strength and local temperature. When including the finite negative effective range, the agreement between theory and experiment becomes *worse* and the free peak shifts to negative values of the rf frequency. This redshift is due to the chemical potential being slightly lower and the system more easily forming molecular pairs.

For the strongly attractive regime in Fig. 9(b), we see the *shifted* spectra match well for the *pairing* peak, but not for the *free* peak, which is strongly renormalized by the chemical potential. The threshold energy is then quite similar: there is closer agreement between the theoretical threshold energy with the finite effective range and the experimental threshold energy. If we take the ratio of the difference of the theoretically determined free and threshold energies to the binding energy we would find that for this interaction and temperature we are also in the pseudogap regime, which we would not expect. This is most likely due to the global chemical potential being negative for large interaction strengths, making the free peak shift to negative frequencies [56]. It is well known that for a large negative chemical potential the Fermi surface is breaking down and two-body bound pairs can form for any binding energy and we are actually not in the pseudogap regime. In this regime the BCS pairing picture gives a fictitious pairing gap as the chemical potential is the gap [5]. In the experiment in order to measure the free peak they introduce a population imbalance, which creates a broader free peak structure, we do not consider this imbalance in this paper, as in the experiment it is only used as a tool to measure the pairing. Experimentally the free peak is then centered around zero rf frequency.

The comparison of our theoretical results of the rf spectra with and without effective range to the experimental data suggests that we can hardly follow the experimental procedure to reliably determine the pseudogap regime, by using the theoretically simulated rf spectra. This is partly due to the fact that for rf spectra the many-body T matrix becomes less accurate in the strongly correlated regime where $\varepsilon_B \sim \varepsilon_F$. The comparison between theory and experiment is further complicated by the fact that, in the current treatment, our theory fails to account for the final-state effect. Thus, at this stage it seems more reliable for us to theoretically determine the pseudogap regime using the specific heat at constant volume.

In Fig. 10, we replot the phase diagram for the pseudogap regime found from the specific heat at constant volume at zero effective range and compare it to the experimental result [see, e.g., Fig. 4(b) in Ref. [21]]. Here, we do not consider the effective range, since the effect of the effective range does not unambiguously show up in the rf spectra as we have just discussed. From the figure, we see that the experimental result at $T \sim 0.5T_F$ agrees well with the predicted pseudogap regime. Experimentally the confinement-induced effective range $k_F^2 R_s$ changes as a function of the binding energy and trap temperature, so it is difficult to have a defined effective range for the entire crossover regime. We would expect that not considering a finite negative effective range to be reasonable in the weakly interacting regime and as the binding energy increases we would expect the negative confinement-induced effective range to become more important and shift the upper and lower bounds of the pseudogap transition towards smaller binding energies.
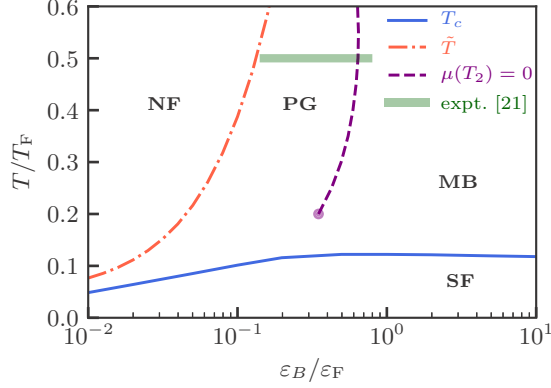
FIG. 10. Pseudogap transition temperature phase diagram plotted as a function of binding energy and reduced temperature. The red dot-dashed curve is the specific-heat prediction, purple dashed is the curve where the chemical potential becomes negative, and the blue solid curve is the BKT transition temperature from the GPF calculation, which are in units of the homogeneous Fermi temperature and energy.

V. CONCLUSIONS

In summary, we have explored the pseudogap regime of a strongly interacting Fermi gas confined to two dimensions with and without a negative confinement-induced effective range. Using the specific heat at constant volume as a probe for high-temperature many-body pairing we have found that in two dimensions it can be used to determine a good characteristic pseudogap formation temperature when compared to the traditional method of defining the pseudogap regime through a suppression in the density of states. We have seen that, as the effective range increases in absolute value, the pseudogap regime shifts to weaker binding energies as the system more preferentially forms pairs.

By comparing our calculations to the recent experiment of Ref. [21], we have obtained good qualitative agreement. Plotting directly the measured in-trap radio-frequency spectra, we have shown our results match well the experimental data in the pseudogap regime, and in the strongly correlated regime the differences can be understood. We have also shown that at high temperatures the many-body pairing regime experimentally defined through radio-frequency measurements fits well with the pseudogap regime theoretically determined from the specific heat at constant volume. However, under the current experimental conditions, it seems difficult to clearly discriminate the effect of the confinement-induced effect range in the radio-frequency spectra and on the pseudogap window, largely due to the insufficient theoretical accuracy for the radio-frequency spectra and insufficient experimental resolution.

APPENDIX: TWO-BODY SCATTERING

Here, we solve the two-particle problem and renormalize the threshold detuning ν. For this purpose, we seek to write the detuning ν and the channel coupling g_b in terms of physical observables, by comparing the two-body T matrix to the quasi-2D scattering amplitude. The two-body T matrix in vacuum is ($E^+ \equiv k^2/M + i0^+$)

$$T_{2B}^{-1}(E^+) = U_{\text{eff}}^{-1}(E^+) + \sum_{\mathbf{p}} \frac{1}{2\epsilon_{\mathbf{p}} - E^+}, \qquad (A1)$$

where $\epsilon_{\mathbf{p}} \equiv \hbar^2 \mathbf{p}^2/(2M)$ and the effective interaction in the presence of the channel coupling is given by

$$U_{\text{eff}}(E^+) = \frac{g_b^2}{E^+ - \nu}. \qquad (A2)$$

Using a large momentum cutoff $\Lambda \to \infty$ in the integral, we find that

$$T_{2B}^{-1}(E^+) = \frac{k^2/M - \nu}{g_b^2} + \frac{M}{4\pi}\left(\ln\left[\frac{\Lambda^2 - k^2}{k^2}\right] + i\pi\right). \quad (A3)$$

In the limit of $k \to 0$, we would have $T_{2B}(E^+) = (\hbar^2/M)f_{Q2D}(k)$. Thus, we consider the low-energy expansion of the quasi-2D scattering amplitude in [57,58]:

$$f_{Q2D}(k \to 0) = \frac{4\pi}{\sqrt{2\pi}\,a_z/a_{3D} + \varpi\left(k^2 a_z^2/2\right)}, \qquad (A4)$$

where $a_z \equiv \sqrt{1/(M\omega_z)}$ is the harmonic oscillator length, a_{3D} is the three-dimensional s-wave scattering length, and the function $\varpi(x)$ has the form $\varpi(x \to 0) \simeq -\ln(2\pi x/\mathcal{B}) + 2x\ln 2 + i\pi$ for $\mathcal{B} = 0.9049$. This leads to

$$T_{2B}(E^+) = \frac{m}{4\pi}(-2\ln[ka_s] - R_s k^2 + i\pi), \qquad (A5)$$

where $a_s \equiv a_z\sqrt{\pi/\mathcal{B}}\exp(-\sqrt{\pi/2}a_z/a_{3D})$ is the 2D s-wave scattering length and the detuning and Feshbach coupling satisfy

$$a_s = \frac{1}{\Lambda}e^{\frac{2\pi\nu}{g_b M}}, \qquad R_s = -\frac{4\pi\hbar^4}{M^2}\frac{1}{g_b^2}. \qquad (A6)$$

We remove the cutoff Λ by considering the pole of the two-body T matrix $T_{2B}(E)$, $E = E_B$, finding that

$$\nu = E_B + g_b^2 \sum_{\mathbf{k}} \frac{1}{2\epsilon_{\mathbf{k}} - E_B}. \qquad (A7)$$

The binding energy can be set by $\varepsilon_B = -E_B = \kappa^2/M$ where we have set $k \to i\kappa$. The effective interaction strength is then

$$\frac{1}{U_{\text{eff}}} = -\sum_{\mathbf{k}} \frac{1}{2\epsilon_{\mathbf{k}} + \varepsilon_B} - \frac{M^2 R_s}{4\pi}\left(i\nu_n - \frac{\epsilon_{\mathbf{q}}}{2} + 2\mu + \varepsilon_B\right). \qquad (A8)$$

[1] V. M. Loktev, R. M. Quick, and S. G. Sharapov, Phase fluctuations and pseudogap phenomena, Phys. Rep. **349**, 1 (2001).

[2] Q. Chen, J. Stajic, S. Tan, and K. Levin, BCS–BEC crossover: From high temperature superconductors to ultracold superfluids, Phys. Rep. **412**, 1 (2005).

[3] J. Stajic, Making sense of the cuprate pseudogap, Science **357**, 561 (2017).

[4] C.-C. Chien, H. Guo, Y. He, and K. Levin, Comparative study of BCS-BEC crossover theories above T_c: The nature of the pseudogap in ultracold atomic Fermi gases, Phys. Rev. A **81**, 023622 (2010).

[5] E. J. Mueller, Review of pseudogaps in strongly interacting fermi gases, Rep. Prog. Phys. **80**, 104401 (2017).

[6] J. P. Gaebler, J. T. Stewart, T. E. Drake, D. S. Jin, A. Perali, P. Pieri, and G. C. Strinati, Observation of pseudogap behaviour in a strongly interacting Fermi gas, Nat. Phys. **6**, 569 (2010).

[7] Päivi Törmä, Physics of ultracold Fermi gases revealed by spectroscopies, Phys. Scr. **91**, 043006 (2016).

[8] R. Haussmann, M. Punk, and W. Zwerger, Spectral functions and rf response of ultracold fermionic atoms, Phys. Rev. A **80**, 063612 (2009).

[9] S. Tsuchiya, R. Watanabe, and Y. Ohashi, Single-particle properties and pseudogap effects in the BCS-BEC crossover regime of an ultracold Fermi gas above T_c, Phys. Rev. A **80**, 033613 (2009).

[10] H. Hu, X.-J. Liu, P. D. Drummond, and H. Dong, Pseudogap Pairing in Ultracold Fermi Atoms, Phys. Rev. Lett. **104**, 240407 (2010).

[11] A. Perali, F. Palestini, P. Pieri, G. C. Strinati, J. T. Stewart, J. P. Gaebler, T. E. Drake, and D. S. Jin, Evolution of the Normal State of a Strongly Interacting Fermi Gas from a Pseudogap Phase to a Molecular Bose Gas, Phys. Rev. Lett. **106**, 060402 (2011).

[12] M. Bauer, M. M. Parish, and T. Enss, Universal Equation of State and Pseudogap in the Two-Dimensional Fermi Gas, Phys. Rev. Lett. **112**, 135302 (2014).

[13] J. Kinast, A. Turlapov, J. E. Thomas, Q. Chen, J. Stajic, and K. Levin, Heat capacity of a strongly interacting Fermi gas, Science **307**, 1296 (2005).

[14] P. van Wyk, H. Tajima, R. Hanai, and Y. Ohashi, Specific heat and effects of pairing fluctuations in the BCS-BEC-crossover regime of an ultracold Fermi gas, Phys. Rev. A **93**, 013621 (2016).

[15] K. Martiyanov, V. Makhalov, and A. Turlapov, Observation of a Two-Dimensional Fermi Gas of Atoms, Phys. Rev. Lett. **105**, 030404 (2010).

[16] M. Feld, B. Frohlich, E. Vogt, M. Koschorreck, and M. Kohl, Observation of a pairing pseudogap in a two-dimensional Fermi gas, Nature (London) **480**, 75 (2011).

[17] B. Fröhlich, M. Feld, E. Vogt, M. Koschorreck, W. Zwerger, and M. Köhl, Radio-Frequency Spectroscopy of a Strongly Interacting Two-Dimensional Fermi Gas, Phys. Rev. Lett. **106**, 105301 (2011).

[18] Y. Zhang, W. Ong, I. Arakelyan, and J. E. Thomas, Polaron-To-Polaron Transitions in the Radio-Frequency Spectrum of a Quasi-Two-Dimensional Fermi Gas, Phys. Rev. Lett. **108**, 235302 (2012).

[19] R. Watanabe, S. Tsuchiya, and Y. Ohashi, Low-dimensional pairing fluctuations and pseudogapped photoemission spectrum in a trapped two-dimensional Fermi gas, Phys. Rev. A **88**, 013637 (2013).

[20] F. Marsiglio, P. Pieri, A. Perali, F. Palestini, and G. C. Strinati, Pairing effects in the normal phase of a two-dimensional Fermi gas, Phys. Rev. B **91**, 054509 (2015).

[21] P. A. Murthy, M. Neidig, R. Klemt, L. Bayha, I. Boettcher, T. Enss, M. Holten, G. Zürn, P. M. Preiss, and S. Jochim, High-temperature pairing in a strongly interacting two-dimensional Fermi gas, Science **359**, 452 (2018).

[22] G. Bertaina and S. Giorgini, BCS-BEC Crossover in a Two-Dimensional Fermi Gas, Phys. Rev. Lett. **106**, 110403 (2011).

[23] L. He, H. Lü, G. Cao, H. Hu, and X.-J. Liu, Quantum fluctuations in the BCS-BEC crossover of two-dimensional Fermi gases, Phys. Rev. A **92**, 023620 (2015).

[24] L. M. Schonenberg, P. C. Verpoort, and G. J. Conduit, Effective-range dependence of two-dimensional Fermi gases, Phys. Rev. A **96**, 023619 (2017).

[25] B. C. Mulkerin, L. He, P. Dyke, C. J. Vale, X.-J. Liu, and H. Hu, Superfluid density and critical velocity near the Berezinskii-Kosterlitz-Thouless transition in a two-dimensional strongly interacting Fermi gas, Phys. Rev. A **96**, 053608 (2017).

[26] Y.-Y. He, H. Shi, and S. Zhang, Reaching the Continuum Limit in Finite-Temperature *Ab Initio* Field-Theory Computations in Many-Fermion Systems, Phys. Rev. Lett. **123**, 136402 (2019).

[27] S. N. Klimin, J. Tempere, and J. T. Devreese, Pseudogap and preformed pairs in the imbalanced Fermi gas in two dimensions, New J. Phys. **14**, 103044 (2012).

[28] B. C. Mulkerin, K. Fenech, P. Dyke, C. J. Vale, X.-J. Liu, and H. Hu, Comparison of strong-coupling theories for a two-dimensional Fermi gas, Phys. Rev. A **92**, 063636 (2015).

[29] M. Matsumoto and Y. Ohashi, Pseudogap phenomena in a two-dimensional ultracold Fermi gas near the Berezinskii-Kosterlitz-Thouless transition, J. Phys. Conf. Ser. **568**, 012012 (2014).

[30] E. R. Anderson and J. E. Drut, Pressure, Compressibility, and Contact of the Two-Dimensional Attractive Fermi Gas, Phys. Rev. Lett. **115**, 115301 (2015).

[31] M. Holten, L. Bayha, A. C. Klein, P. A. Murthy, P. M. Preiss, and S. Jochim, Anomalous Breaking of Scale Invariance in a Two-Dimensional Fermi Gas, Phys. Rev. Lett. **121**, 120401 (2018).

[32] T. Peppler, P. Dyke, M. Zamorano, I. Herrera, S. Hoinka, and C. J. Vale, Quantum Anomaly and 2D-3D Crossover in Strongly Interacting Fermi Gases, Phys. Rev. Lett. **121**, 120402 (2018).

[33] P. A. Murthy, N. Defenu, L. Bayha, M. Holten, P. M. Preiss, T. Enss, and S. Jochim, Quantum scale anomaly and spatial coherence in a 2D Fermi superfluid, Science **365**, 268 (2019).

[34] J. Hofmann, Quantum Anomaly, Universal Relations, and Breathing Mode of a Two-Dimensional Fermi Gas, Phys. Rev. Lett. **108**, 185303 (2012).

[35] C. Gao and Z. Yu, Breathing mode of two-dimensional atomic Fermi gases in harmonic traps, Phys. Rev. A **86**, 043609 (2012).

[36] B. C. Mulkerin, X.-J. Liu, and H. Hu, Collective modes of a two-dimensional Fermi gas at finite temperature, Phys. Rev. A **97**, 053612 (2018).

[37] U. Toniolo, B. C. Mulkerin, X.-J. Liu, and H. Hu, Breathing-mode frequency of a strongly interacting Fermi gas across the two- to three-dimensional crossover, Phys. Rev. A **97**, 063622 (2018).

[38] H. Hu, B. C. Mulkerin, U. Toniolo, L. He, and X.-J. Liu, Reduced Quantum Anomaly in a Quasi-Two-Dimensional Fermi Superfluid: Significance of the Confinement-Induced Effective Range of Interactions, Phys. Rev. Lett. **122**, 070401 (2019).

[39] J. P. Kestner and L.-M. Duan, Effective low-dimensional hamiltonian for strongly interacting atoms in a transverse trap, Phys. Rev. A **76**, 063610 (2007).

[40] A. M. Fischer and M. M. Parish, BCS-BEC crossover in a quasi-two-dimensional Fermi gas, Phys. Rev. A **88**, 023612 (2013).

[41] F. Wu, J. Hu, L. He, X.-J. Liu, and H. Hu, Effective theory for ultracold strongly interacting fermionic atoms in two dimensions, Phys. Rev. A **101**, 043607 (2020).

[42] J. Levinsen and M. M. Parish, Bound States in a Quasi-Two-Dimensional Fermi Gas, Phys. Rev. Lett. **110**, 055304 (2013).

[43] Y. Ohashi and A. Griffin, BCS-BEC Crossover in a Gas of Fermi Atoms with a Feshbach Resonance, Phys. Rev. Lett. **89**, 130402 (2002).

[44] V. Gurarie and L. Radzihovsky, Resonantly paired fermionic superfluids, Ann. Phys. (NY) **322**, 2 (2007), january Special Issue 2007.

[45] H. Tajima, Precursor of superfluidity in a strongly interacting Fermi gas with negative effective range, Phys. Rev. A **97**, 043613 (2018).

[46] B. C. Mulkerin, H. Hu, and X.-J. Liu, Role of the confinement-induced effective range in the thermodynamics of a strongly correlated Fermi gas in two dimensions, Phys. Rev. A **101**, 013605 (2020).

[47] X.-J. Liu and H. Hu, Self-consistent theory of atomic Fermi gases with a Feshbach resonance at the superfluid transition, Phys. Rev. A **72**, 063613 (2005).

[48] V. Pietilä, Pairing and radio-frequency spectroscopy in two-dimensional Fermi gases, Phys. Rev. A **86**, 023608 (2012).

[49] M. Veillette, E. G. Moon, A. Lamacraft, L. Radzihovsky, S. Sachdev, and D. E. Sheehy, Radio-frequency spectroscopy of a strongly imbalanced Feshbach-resonant Fermi gas, Phys. Rev. A **78**, 033614 (2008).

[50] D. Rohe and W. Metzner, Pair-fluctuation-induced pseudogap in the normal phase of the two-dimensional attractive Hubbard model at weak coupling, Phys. Rev. B **63**, 224509 (2001).

[51] P. Nozieres and S. Schmitt-Rink, Bose condensation in an attractive fermion gas: From weak to strong coupling superconductivity, J. Low Temp. Phys. **59**, 195 (1985).

[52] P. C. Hohenberg, Existence of long-range order in one and two dimensions, Phys. Rev. **158**, 383 (1967).

[53] R. M. May, Quantum statistics of ideal gases in two dimensions, Phys. Rev. **135**, A1515 (1964).

[54] P. Massignan, G. M. Bruun, and H. T. C. Stoof, Spin polarons and molecules in strongly interacting atomic Fermi gases, Phys. Rev. A **78**, 031602(R) (2008).

[55] See the Appendix of Ref. [14] for details on the calculation of N_B.

[56] M. Barth and J. Hofmann, Pairing effects in the nondegenerate limit of the two-dimensional Fermi gas, Phys. Rev. A **89**, 013614 (2014).

[57] D. S. Petrov and G. V. Shlyapnikov, Interatomic collisions in a tightly confined Bose gas, Phys. Rev. A **64**, 012706 (2001).

[58] I. Bloch, J. Dalibard, and W. Zwerger, Many-body physics with ultracold gases, Rev. Mod. Phys. **80**, 885 (2008).